The Astrophysical Journal, 766:41 (12pp), 2013 March 20 doi:10.1088/0004-637X/766/1/41

IDENTIFYING THE LOCATION IN THE HOST GALAXY OF THE SHORT GRB 111117A WITH THE *CHANDRA* SUBARCSECOND POSITION

T. Sakamoto[1,2,3,4], E. Troja[1,3,5,26], K. Aoki[6], S. Guiriec[3,26], M. Im[7], G. Leloudas[8,9], D. Malesani[8], A. Melandri[10], A. de Ugarte Postigo[8,11], Y. Urata[12], D. Xu[13], P. D'Avanzo[10], J. Gorosabel[11], Y. Jeon[7], R. Sánchez-Ramírez[11], M. I. Andersen[8,14], J. Bai[15,16], S. D. Barthelmy[3], M. S. Briggs[17], S. Foley[18], A. S. Fruchter[19], J. P. U. Fynbo[8], N. Gehrels[3], K. Huang[20], M. Jang[7], N. Kawai[21], H. Korhonen[14,22], J. Mao[15,16,23], J. P. Norris[24], R. D. Preece[17], J. L. Racusin[3], C. C. Thöne[11], K. Vida[25], and X. Zhao[15,16]

[1] Center for Research and Exploration in Space Science and Technology (CRESST), NASA Goddard Space Flight Center, Greenbelt, MD 20771, USA
[2] Joint Center for Astrophysics, University of Maryland, Baltimore County, 1000 Hilltop Circle, Baltimore, MD 21250, USA
[3] NASA Goddard Space Flight Center, Greenbelt, MD 20771, USA
[4] Department of Physics and Mathematics, College of Science and Engineering, Aoyama Gakuin University, 5-10-1 Fuchinobe, Chuo-ku, Sagamihara-shi, Kanagawa 252-5258, Japan
[5] Joint Center for Astrophysics, Department of Astronomy, University of Maryland College Park, MD 20742-2421, USA
[6] Subaru Telescope, National Astronomical Observatory of Japan, 650 North A'ohoku Place, Hilo, HI 96720, USA
[7] Center for the Exploration of the Origin of the Universe (CEOU), Department of Physics and Astronomy, Seoul National University, Seoul, 151-747, Republic of Korea
[8] Dark Cosmology Centre, Niels Bohr Institute, University of Copenhagen, Juliane Maries Vej 30, DK-2100 Copenhagen Ø, Denmark
[9] The Oskar Klein Centre, Department of Physics, Stockholm University, SE-106 91 Stockholm, Sweden
[10] INAF-Osservatorio Astronomico di Brera, via Bianchi 46, I-23807 Merate (LC), Italy
[11] Instituto de Astrofísica de Andalucía (CSIC), Glorieta de la Astronomía s/n, E-18008 Granada, Spain
[12] Institute of Astronomy, National Central University, Chung-Li 32054, Taiwan
[13] Department of Particle Physics and Astronomy, The Weizmann Institute of Science, Rehovot 76100, Israel
[14] Niels Bohr Institute, University of Copenhagen, Juliane Maries Vej 30, DK-2100 Copenhagen, Denmark
[15] Yunnan Astronomical Observatory, Chinese Academy of Sciences, Kunming, Yunnan Province, 650011, China
[16] Key Laboratory for the Structure and Evolution of Celestial Objects, Chinese Academy of Sciences, Kunming, 650011, China
[17] Center for Space Plasma and Aeronomic Research, University of Alabama in Huntsville, 320 Sparkman Drive, Huntsville, AL 35805, USA
[18] Max-Planck-Institut für extraterrestrische Physik, Giessenbachstrasse 1, D-85748 Garching, Germany
[19] Space Telescope Science Institute, 3700 San Martin Drive, Baltimore, MD 21218, USA
[20] Academia Sinica Institute of Astronomy and Astrophysics, Taipei 106, Taiwan
[21] Department of Physics, Tokyo Institute of Technology, 2-12-1 Ookayama, Meguro-ku, Tokyo 152-8551, Japan
[22] Centre for Star and Planet Formation, Natural History Museum of Denmark, University of Copenhagen, Øster Voldgade 5-7, DK-1350 Denmark
[23] Space Science Division, Korea Astronomy and Space Science Institute, 776, Daedeokdae-ro, Yuseong-gu, Daejeon, 305-348, Republic of Korea
[24] Physics Department, Boise State University, 1910 University Drive, Boise, ID 83725, USA
[25] Konkoly Observatory of the Hungarian Academy of Sciences, Konkoly Thege út 15-17, 1121, Budapest XII, Hungary
Received 2012 May 29; accepted 2013 January 4; published 2013 March 6

ABSTRACT

We present our successful *Chandra* program designed to identify, with subarcsecond accuracy, the X-ray afterglow of the short GRB 111117A, which was discovered by *Swift* and *Fermi*. Thanks to our rapid target of opportunity request, *Chandra* clearly detected the X-ray afterglow, though no optical afterglow was found in deep optical observations. The host galaxy was clearly detected in the optical and near-infrared band, with the best photometric redshift of $z = 1.31^{+0.46}_{-0.23}$ (90% confidence), making it one of the highest known short gamma-ray burst (GRB) redshifts. Furthermore, we see an offset of 1.0 ± 0.2 arcsec, which corresponds to 8.4 ± 1.7 kpc, between the host and the afterglow position. We discuss the importance of using *Chandra* for obtaining subarcsecond X-ray localizations of short GRB afterglows to study GRB environments.

Key word: gamma-ray burst: individual (GRB 111117A)

Online-only material: color figures

1. INTRODUCTION

Gamma-ray bursts (GRBs) are traditionally divided into two classes based on their duration and spectral hardness: the long duration/soft spectrum GRBs, and the short duration/hard spectrum GRBs (Kouveliotou et al. 1993). The two classes of bursts further differ in their spectral lags, the measurement of the delay in the arrival time of the low-energy photons with respect to the higher energy ones: long bursts tend to have large positive lags, while short bursts exhibit negligible or negative lags (Norris & Bonnell 2006). The long-standing paradigm is that these two phenomenological classes of GRBs originate from different progenitor systems. A preponderance of evidence now links long GRBs with the death of massive stars (Woosley & Bloom 2006, and references therein), yet the origin of short GRBs remains largely unknown. The common notion that short bursts originate from coalescing compact binaries, either neutron star–neutron star (NS–NS) or neutron star–black hole (NS–BH) mergers (e.g., Eichler et al. 1989; Paczynski 1991; Narayan et al. 1992; Rosswog 2005; Rezzolla et al. 2011), makes them the most promising tool to aid in the direct detection of gravitational waves (GWs) by forthcoming facilities such as Advanced-LIGO, Advanced-VIRGO, or LCGT (KAGRA) (e.g., Nissanke et al. 2010). It is therefore of primary importance to convincingly corroborate the merger scenario with a robust observational basis.

[26] NASA Postdoctoral Program Fellow.

Significant progress in understanding the origin of short GRBs has been achieved only recently. This advance was enabled by the detection of their afterglows in 2005 thanks to the rapid position notice and response by *HETE-2* (Ricker et al. 2003) and *Swift* (Gehrels et al. 2004). The very first localizations of short GRBs immediately provided us with fundamental clues about their nature. They demonstrated that short GRBs are cosmological events with an isotropic equivalent energy scale of 10^{49}–10^{52} erg, that they occur in different environments than long GRBs, and are not associated with bright Type Ic supernovae (Bloom et al. 2006; Prochaska et al. 2006; Covino et al. 2006).

Since 2005 the sample of well-localized short GRBs has significantly grown, allowing for a deeper insight into the nature of their progenitors. The observed redshift distribution, ranging $0.11 \lesssim z \lesssim 1$, hints at a progenitor system with a broad range of lifetimes (Berger et al. 2007). Another critical test of the progenitor models is the observed offset distribution of short bursts (Troja et al. 2008; Fong et al. 2010; Church et al. 2011). The median physical projected offset between the host center and the short GRB position is ∼5 kpc (Fong et al. 2010), which is about five times larger than that of long GRBs (Bloom et al. 2002), and shows a broader dispersion. This is in agreement with the merger scenario, as several models NS–NS/NS–BH systems are expected to receive significant kick velocities at birth (Bloom et al. 1999; Fryer et al. 1999; Belczynski et al. 2006), or to dynamically form in globular clusters in the outskirts of their galaxies (Grindlay et al. 2006).

Despite the major progress of the last few years, the study of short GRBs and their progenitors has still been suffering from their less secure afterglow positions and redshifts. Unlike long GRBs, none of the redshifts of short GRBs[27] has been directly measured through afterglow spectroscopy, and only in the case of GRB 060121, was a photometric redshift derived from the afterglow spectral energy distribution (de Ugarte Postigo et al. 2006; Levan et al. 2006). This is because the optical afterglows are significantly fainter than those of long GRBs (Nysewander et al. 2009; Kann et al. 2011). The redshifts of short GRBs are instead measured from spectroscopic observations of the "associated" host galaxy. The likelihood of a spurious association is small when a subarcsecond position is available. However, if an afterglow is only detected by the *Swift* X-Ray Telescope (XRT; Burrows et al. 2005), the probability of a chance alignment is higher due to the larger uncertainty in the localization (2″–5″). Unfortunately, the latter scenario represents the majority of cases (∼65% of the *Swift* short bursts sample).

A further bias is introduced by the fact that subarcsecond positions are mainly derived from optical afterglow detections, which are subject both to absorption along the line of sight and density effects. In fact, in the standard fireball model, the optical brightness depends sensitively on the density of the circumburst environment (Kumar & Panaitescu 2000). This effect disfavors the accurate localization of short GRBs occurring in the lower-density galaxy halo or even outside their own galaxy, in the intergalactic medium. Such populations of large-offset short GRBs has already been suggested by Bloom et al. (2007) and Troja et al. (2008). However, being localized mainly by XRT, their association with the putative host galaxy remains uncertain. Increasing the sample of large-offset short bursts with subarcsecond localization is crucial to determine whether their progenitors were ejected from their birth site, favoring models that predict NS binaries with large kick velocities and ∼Gyr lifetimes, or were formed from dynamical interactions in globular clusters (Salvaterra et al. 2010).

In this context, rapid *Chandra* observations of short GRB afterglows represent the critical observational gateway to overcome the current observational limits. Since 65% of *Swift* short GRBs are detected in X-rays, and only 25% of them are detected in the optical band, X-ray observations have a higher probability of detecting the afterglows of short GRBs. The superb angular resolution of *Chandra* allows for a subarcsecond localization, comparable to optical localizations, thus enabling the secure host identification and the precise measurement of the GRB projected offset. Furthermore, because the X-ray afterglow is less subject to absorption and density effects, *Chandra* localizations allow us to build a sample of well-localized short GRBs with limited bias, complementing the information derived from the sample of optically localized short GRBs. This is the key to distinguishing between the different possible short GRB populations (Sakamoto & Gehrels 2009), which could arise from a different progenitor and/or environment.

In this paper, we report the first results of our *Chandra* program which led to the accurate localization of GRB 111117A detected by *Swift* and *Fermi*. GRB 111117A is the second short burst[28] in which the *Chandra* position is crucial for the host identification. Our results were leveraged with an intense ground-based follow-up campaign. No optical/infrared counterpart was found, therefore our *Chandra* localization uniquely provides the only accurate subarcsecond position. The paper is organized as follows. We introduce GRB 111117A in Section 2. In Section 3, we describe the analysis software and methods used in this paper. We report the prompt emission properties in Section 4, the X-ray afterglow properties in Section 5.1, the deep optical afterglow limits in Section 5.2, and the host galaxy properties in Section 6. We discuss and summarize our results in Section 7. The quoted errors are at the 90% confidence level for prompt emission and X-ray afterglow data, and at the 68% confidence level for optical and near-infrared data unless stated otherwise. The reported optical and near-infrared magnitudes are in the Vega system unless stated otherwise. Throughout the paper, we use the cosmological parameters, $\Omega_m = 0.27$, $\Omega_\Lambda = 0.73$, and $H_0 = 71\ \mathrm{km\ s^{-1}\ Mpc^{-1}}$.

2. GRB 111117A

On 2011 November 17 at 12:13:41.921 UT, the *Swift* Burst Alert Telescope (BAT; Barthelmy et al. 2005) triggered and localized the short GRB 111117A (Mangano et al. 2011). The *Fermi* Gamma-Ray Burst Monitor (GBM; Meegan et al. 2009) also triggered on the burst (Foley et al. 2011). The BAT location derived from the ground analysis was (R.A., Decl.) (J2000) = ($00^{\mathrm{h}}50^{\mathrm{m}}49\overset{\mathrm{s}}{.}4$, $+23^\circ00'36''$) with a 90% error radius of 1′.8. The *Swift* XRT started its observation 76.8 s after the trigger. A fading X-ray source was found at the location of (R.A., Decl.) (J2000) = ($00^{\mathrm{h}}50^{\mathrm{m}}46\overset{\mathrm{s}}{.}22$, $+23^\circ00'39''.2$) with a 90% error radius of 2″.1 (Melandri et al. 2011b). The *Swift* UV-Optical Telescope (UVOT; Roming et al. 2005) began the observations of the field 137 s after the trigger, and no optical afterglow was detected (Oates & Mangano 2011).

[27] Although the redshift of GRB 090426 (the t_{90} duration measured by BAT is 1.24) has been measured from the absorption spectroscopy (Levesque et al. 2010; Thöne et al. 2011), there is growing observational evidence that the progenitor of this GRB is akin to that of long GRBs (e.g., Xin et al. 2011; Lü et al. 2010).

[28] The first one was GRB 111020A (Fong et al. 2012).

Table 1
Log of Optical and Near-infrared Observations of GRB 111117A

Time Since the Trigger[a] (day)	Telescope	Instrument	Filter	Exposure (s)	Afterglow[b] (mag)	Host[b] (mag)
0.083	GMG	YFOSC YSU	R	600		>22.1
0.104	GMG	YFOSC YSU	z	900		22.9 ± 0.3 (AB)[c]
0.300	TNG	LRS	R	1800	>24.1	23.49 ± 0.29
0.329	GTC	OSIRIS	g	800		24.05 ± 0.14 (AB)
0.342	GTC	OSIRIS	r	1200	>24.9 (AB)	24.17 ± 0.10 (AB)
0.354	GTC	OSIRIS	i	360		23.92 ± 0.20 (AB)
0.358	NOT	ALFOSC	z	3600		>22.5 (AB)
0.371	NOT	ALFOSC	R	3000		23.20 ± 0.25
1.5	NOT	ALFOSC	R	2400		23.26 ± 0.22
11.4	TNG	LRS	R	3600		23.43 ± 0.13
11.8	Subaru	IRCS	K'	780		>19.95
14.4	GTC	OSIRIS	r	2400		24.20 ± 0.07 (AB)
19 – 72[d]	UKIRT	WFCAM	K	8640		20.91 ± 0.12
42.7	CFHT	WIRCam	J	4140		21.7 ± 0.2

Notes. The magnitudes are corrected for Galactic extinction.
[a] The mean time of the stacked observations with the corresponding exposure time.
[b] Upper limit is in 3σ confidence level.
[c] Possible host detection.
[d] UKIRT data were collected at the multiple epochs between 19 and 72 days after the burst.

The earliest ground observations of the field were performed by the Gao-Mei-Gu telescope (GMG) at 1.96 hr after the BAT trigger, and no afterglow was detected within the XRT error circle with an exposure time of 600 s in the R band (Zhao et al. 2011). The Nordic Optical Telescope (NOT) observed the field at 8.9 hr after the burst, and found an optical source inside the XRT error circle (Andersen et al. 2011), which was later confirmed to have a possible extended morphology by the Magellan/Baade telescope (Fong et al. 2011), the Gemini-South telescope (Cucchiara & Cenko 2011), the GROND telescope (Schmidl et al. 2011), and the Telescopio Nazionale Galileo (TNG; Melandri et al. 2011a). The Gran Telescopio CANARIAS (GTC), the Subaru telescope, the United Kingdom Infrared Telescope (UKIRT), and the Canada–France–Hawaii Telescope (CFHT) also collected images of the field.

Based on no clear detection of an optical afterglow of the short GRB 111117A, we triggered our *Chandra* Target of Opportunity (ToO) observation 6 hr after the trigger (Sakamoto et al. 2011b), and the observation started 3 days later. The X-ray afterglow was clearly detected in 20 ks, obtaining a subarcsecond position of the afterglow in X-rays (Sakamoto et al. 2011c).

3. DATA ANALYSIS

HEAsoft version 6.11 and *Swift* CALDB (version 20090130) were used for the *Swift* BAT data analysis. The XRT data products were obtained from the automated results available from the UK *Swift* Science Data Center (Evans et al. 2007, 2009). CIAO 4.3 and CALDB 4.4.6 were used for the *Chandra* data analysis. The *Fermi* GBM data were prepared using the RMFIT software package,[29] with data from three sodium iodide (NaI) scintillation detectors (detector ID 6, 7 and 9) and two bismuth germanate (BGO) scintillation detectors (detector ID 0 and 1).

A standard data reduction of optical and near-infrared images was performed using the IRAF[30] software package. SExtractor[31] (Bertin & Arnouts 1996), SkyCat Gaia[32] and IRAF were used to extract sources and perform the photometry. To accomplish consistent photometry for images collected by various telescopes, we selected 10 common stars in the field and performed relative photometry. When some of the stars were saturated (especially for a large aperture telescope such as GTC), a subset of these 10 reference stars were used. The USNO B-1 R2 magnitude or the Sloan Digital Sky Survey (SDSS) magnitudes were used as the reference magnitude for the stars. For the near-infrared images of UKIRT and CFHT, we use the reference stars in the 2MASS catalog. The Galactic extinction has been corrected using $E(B-V) = 0.03$ mag toward the direction to this burst (Schlegel et al. 1998). The log of optical and near-infrared observations presented in this paper is summarized in Table 1.

4. PROMPT EMISSION

The light curve of the prompt emission is composed of two episodes: the first episode shows multiple overlapping pulses with a total duration of 0.3 s, and the second episode is composed of two pulses with a duration of 0.1 s (Figure 1). The duration is $T_{90} = 464 \pm 54$ ms (1σ error; 15–350 keV) measured using the BAT background-subtracted light curve using the mask modulation (e.g., mask-weighted light curve). This T_{90} duration is significantly shorter than 2 s, which is the standard classification of short GRBs form BATSE (Kouveliotou et al. 1993). Furthermore, this duration is shorter than 0.7 s, which is claimed to be the dividing line between long and short GRBs for the *Swift* sample (Bromberg et al. 2012). The hard-to-soft spectral evolution is seen in both the first and the second episode of GRB 111117A (see the hardness ratio plot at the bottom panel of Figure 1). There is no indication of extended emission (Norris et al. 2011) down to a flux level of $\sim 2 \times 10^{-10}$ erg cm^{-2} s^{-1}, assuming a power-law spectrum with a photon index of $\alpha = -2$ ($N(E) \propto E^{\alpha}$) in the 14–200 keV band by examining the BAT sky image from 60 s (after the spacecraft slew settled) to 950 s after the BAT trigger time

[29] http://fermi.gsfc.nasa.gov/ssc/data/analysis/user/
[30] http://iraf.noao.edu/
[31] http://www.astromatic.net/software/sextractor
[32] http://astro.dur.ac.uk/~pdraper/gaia/gaia.html

Table 2
Time-integrated Spectral Parameters of GRB 111117A

Instrument	Model	α	β	$E_{\rm peak}^{\rm obs}$	C(GBM)	χ^2/dof
BAT	PL	$-0.52^{+0.24}_{-0.22}$	...	...	...	49.5/57 (0.87)
GBM	PL	$-1.44^{+0.06}_{-0.08}$	...	...	...	636.8/604 (1.05)
GBM	CPL	$-0.39^{+0.53}_{-0.37}$	...	440^{+240}_{-125}	...	578.9/603 (0.96)
GBM	Band	$-0.40^{+0.36}_{-0.50}$	<-2.6	450^{+240}_{-125}	...	578.9/602 (0.96)
BAT-GBM	PL	$-1.37^{+0.05}_{-0.07}$	...	...	...	729.5/662 (1.10)
BAT-GBM	CPL	$-0.28^{+0.31}_{-0.26}$	...	420^{+170}_{-110}	$0.62^{+0.16}_{-0.13}$	627.7/661 (0.95)
BAT-GBM	Band	$-0.28^{+0.15}_{-0.26}$	<-2.5	420^{+170}_{-80}	$0.62^{+0.16}_{-0.13}$	627.8/660 (0.95)

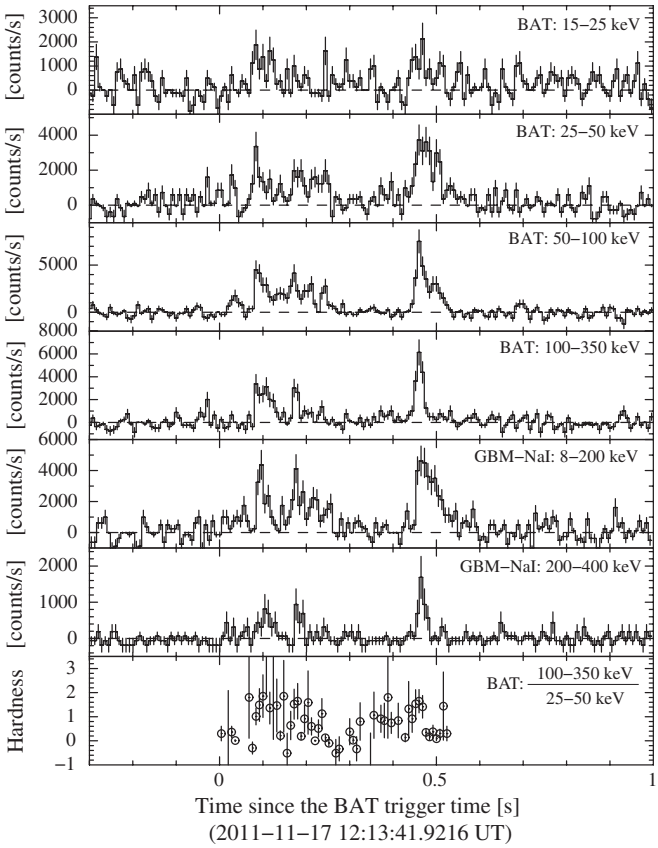

Figure 1. Background-subtracted 5 ms light curves of *Swift* BAT (15–25 keV, 25–50 keV, 50–100 keV, and 100–350 keV) and *Fermi* GBM (8–200 keV and 200–400 keV). The bottom panel shows the hardness ratio between the 100–350 keV and the 25–50 keV of the BAT data.

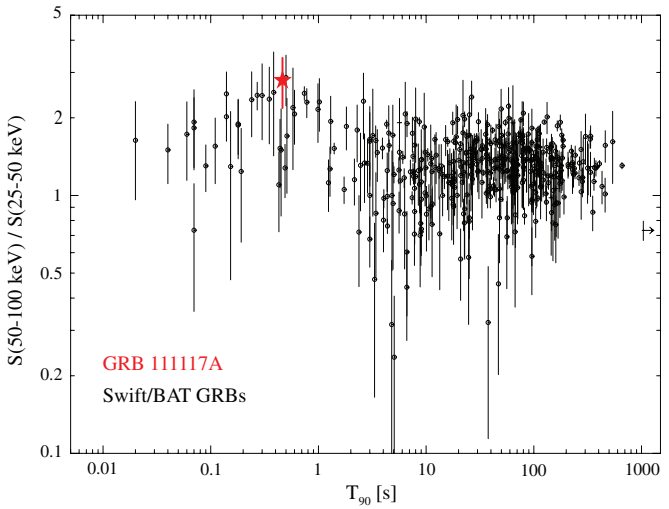

Figure 2. Fluence ratios between the 50–100 keV and the 25–50 keV band vs. T_{90} are shown for GRB 111117A (red) and the *Swift* BAT GRBs. The values of the *Swift* BAT GRBs are extracted from Sakamoto et al. (2011a).
(A color version of this figure is available in the online journal.)

(hereafter $t_{0,\rm BAT}$). The spectral lag between the 100–350 keV and the 25–50 keV band is 0.6 ± 2.4 ms, which is consistent with zero, using the BAT raw light curves (non-mask-weighted light curves) by subtracting a constant background measured around the burst. In the fluence ratio versus T_{90} plane, GRB 111117A is located in the same region where most of the BAT short GRBs are located (Figure 2), further confirming its short GRB nature.

The time-integrated spectral properties are investigated by performing a joint spectral analysis with BAT and GBM data. The spectrum is extracted from $t_{0,\rm BAT}$ + 0.024 s to $t_{0,\rm BAT}$ + 0.520 s using `batbinevt` for the BAT data and using the RMFIT software package for the GBM data in the same time interval. The BAT energy response file is generated by `batdrmgen`. The GBM energy response files were retrieved from the HEASARC *Fermi* archive for trigger bn111117510. We use the `xspec` spectral fitting package to do the joint fit. The energy ranges of 15–150 keV, 8–900 keV, and 0.2–45 MeV are used for the BAT, the GBM-NaI and the GBM-BGO instruments, respectively. The model includes a inter-calibration multiplicative factor to take into account the calibration uncertainty among the different instruments. The best-fit spectral parameters are summarized in Table 2. We find that a power-law multiplied by an exponential cutoff (CPL)[33] provides the best representative model of the data. The best-fit parameters in this model are the power-law photon index $\alpha^{\rm CPL} = -0.28^{+0.31}_{-0.26}$ and $E_{\rm peak} = 420^{+170}_{-110}$ keV (χ^2/dof = 627/661). The 90% confidence interval of the inter-calibration factor of the GBM detectors is between 0.50 and 0.78 which is an acceptable range taking into account the current spectral calibration uncertainty between the BAT and the GBM. A simple power-law model yields a significantly worse fit to the data (χ^2/dof = 729/662). Furthermore, the significant difference in the power-law photon index for the BAT data ($-0.52^{+0.24}_{-0.22}$) and the GBM data ($-1.44^{+0.06}_{-0.08}$) alone disfavors a simple power-law model as the representative model. There is no significant improvement in χ^2 using a Band function (Band et al. 1993) fit (χ^2/dof = 627/660) over a CPL fit. The preferential fit to a CPL model and the systematically harder photon index compared to long GRBs are general characteristics of a time-integrated spectrum of short GRBs

[33] $N(E) \propto E^{\alpha^{\rm CPL}} \exp(-E\,(2+\alpha^{\rm CPL})/E_{\rm peak})$, where $\alpha^{\rm CPL}$ is the power-law photon index and $E_{\rm peak}$ is the peak energy in the νF_ν spectrum.

(e.g., Ghirlanda et al. 2009; Ohno et al. 2008). The fluence in the 8–1000 keV band calculated using the best-fit time-integrated spectral parameters based on a CPL fit above is $7.3^{+2.6}_{-2.1} \times 10^{-7}$ erg cm^{-2}. Due to poor statistics in extracting a spectrum from a very short time window, the peak flux was calculated by scaling the BAT mask-weighted count rate into a flux by folding the BAT energy response and assuming the best-fit time-integrated spectral parameters in a CPL model. The peak energy flux at the 8–1000 keV band in the 50 ms window starting from $t_{0,\mathrm{BAT}}$ + 0.450 s is $(3.8 \pm 1.2) \times 10^{-6}$ erg cm^{-2} s^{-1}. The time-resolved spectroscopy is difficult to perform due to the limited statistics in the data.

We search for pre-burst emission by analyzing the BAT survey data (detector plane histogram, DPH). Approximately 4.5 hr before the burst trigger, GRB 111117A was in the field of view of BAT (26.°1 from the boresight direction) for ∼1 ks during the observation of the blazar PKS 0235+16 (observation ID 00030880085). We use the `batsurvey` script to process the DPH data. The extracted rates at the location of GRB 111117A are corrected to the on-axis rate by applying an off-axis correction based on observations of the Crab. We find no significant emission during this observation at the location of GRB 111117A. The 3σ upper limit assuming a power-law spectrum with a photon index of $\alpha = -2$ is 1.4×10^{-9} erg cm^{-2} s^{-1} at the 14–200 keV band in 300 s exposure.

5. AFTERGLOW

5.1. X-Rays

The *Swift* XRT X-ray afterglow light curve can be fit to a simple power-law decay (Figure 4). The spectrum collected in the photon counting (PC) mode is well described by an absorbed power-law model. The best-fit spectral parameters are a photon index of $-2.19^{+0.36}_{-0.38}$ and an excess N_{H} of $1.8^{+1.1}_{-1.0} \times 10^{21}$ cm^{-2} ($z = 0$) assuming the galactic N_{H} at the burst direction of 3.7×10^{20} cm^{-2} (Kalberla et al. 2005). Both the measured photon index and N_{H} for GRB 111117A are consistent with those of other *Swift* short GRBs (Kopač et al. 2012; Fong et al. 2012).

The *Chandra* observation started at 12:39:25 UT, and ended at 18:39:10 UT on 2011 November 20 with a total exposure of 19.8 ks. The ACIS instrument had five CCD chips (S3, S4, S5, I2, and I3) enabled, with the S3 chip as the aiming point for the source. The data were collected in the FAINT mode. The X-ray afterglow is clearly detected in the *Chandra* observation with 3.9σ significance by `wavdetect` (source net counts of 8) within the XRT error circle. To refine the astrometry of the *Chandra* data, we apply the same analysis method described in Feng & Kaaret (2008). We extract the *Chandra* image (0.35–8 keV) that overlaps with the GTC image (4.′4 × 8.′7). The astrometry of the GTC image is calibrated against the SDSS catalog, and its standard deviation is ∼0.″3. We run `wavdetect` with options of scales = "1.0 2.0 4.0 8.0 16.0" and sigthresh = 4×10^{-6} to the extracted *Chandra* image. There are four sources which have a good match between the images. We then use the `geomap` task in the IRAF IMMATCH package to find the best coordinate transformation between the *Chandra* and the GTC image by fitting those four sources. Finally, we apply `geoxytrans` task (IRAF IMMATCH package) for the originally detected *Chandra* position using the coordinate transformation calculated by `geomap` to find the astrometrically corrected *Chandra* afterglow position. The refined afterglow position is shifted by δR.A. = −0.″221 and δDecl. = −0.″020 from the position originally derived by `wavdetect`. The best *Chandra* X-ray afterglow position is (R.A., Decl.) (J2000) = ($00^{\mathrm{h}}50^{\mathrm{m}}46^{\mathrm{s}}.264$, +23°00′39.″98) with 1$\sigma$ statistical uncertainty of 0.″09 in right ascension and 0.″16 in declination. When we include the systematic uncertainty of 0.″3, 1σ error radius of the *Chandra* position is 0.″35. The *Chandra* position is well within the XRT 90% error circle (see Figure 3).

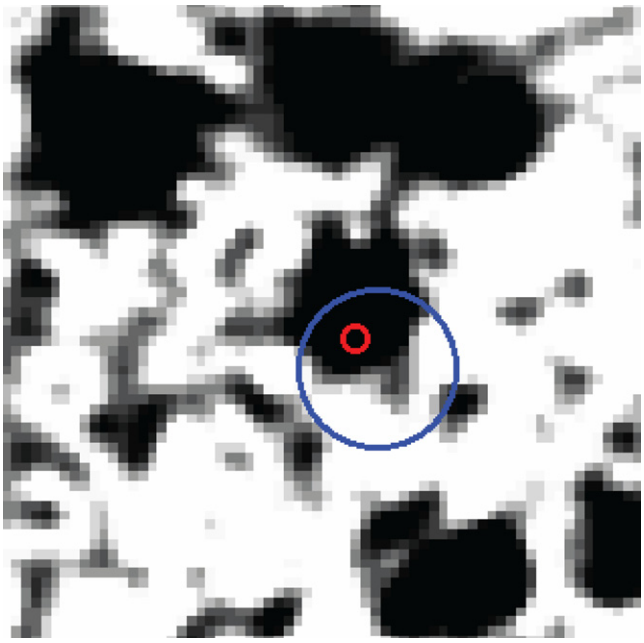

Figure 3. GTC r image (17″ × 17″) with the XRT 90% error circle in blue and the *Chandra* 1σ error circle, which includes the statistical and the systematic error, in red.

(A color version of this figure is available in the online journal.)

The combined *Swift* XRT and *Chandra* X-ray afterglow light curve is well fit by a simple power-law with index of $-1.25^{+0.09}_{-0.12}$. As shown in Figure 4, the X-ray afterglow of GRB 111117A belongs to a dim population of the *Swift* short GRBs.

5.2. Optical

We investigate the possible optical afterglow emission by using the image subtraction technique between the early and the late time epoch observations by TNG and GTC. We use the ISIS software package (Alard & Lupton 1998) to perform the image subtraction. The early and the late epoch observations of TNG and GTC were obtained at $t_{0,\mathrm{BAT}}$ + 7.23 hr and $t_{0,\mathrm{BAT}}$ + 7.89 hr, and $t_{0,\mathrm{BAT}}$ + 11.4 days and $t_{0,\mathrm{BAT}}$ + 14.4 days, respectively. We find no significant emission at the *Chandra* X-ray afterglow location in the subtracted images in both the TNG and the GTC observations (Figure 5), with 3σ upper limits of $R > 24.1$ mag for TNG and $r > 24.9$ (AB) mag for GTC. The TNG limiting magnitudes of the first and second epochs are $R > 24.7$ mag and $R > 25.4$ mag, respectively. For GTC, the limiting magnitude of the first and second epoch are $r > 25.8$ (AB) mag and $r > 26.1$ (AB) mag, respectively. Those limits are some of the deepest optical limits on short GRBs ever obtained (see upper panel of Figure 6).

6. HOST GALAXY

The host galaxy of GRB 111117A has been detected in the near infrared and optical bands. There is only one near-infrared/optical source located near the *Chandra* X-ray afterglow position. Although the weak nature of the source makes

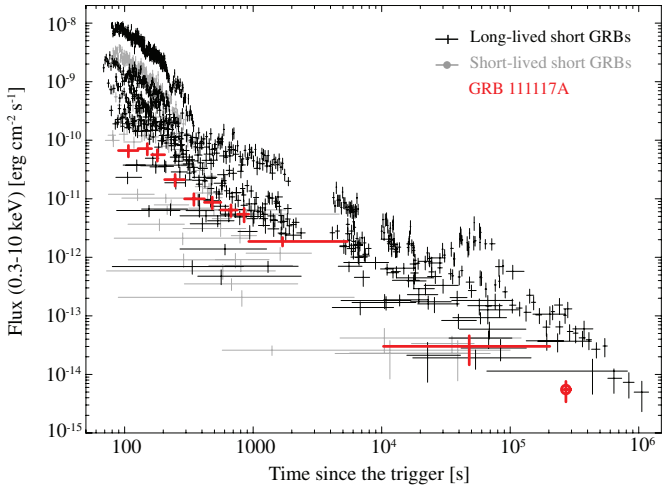

Figure 4. Comparison of X-ray afterglow light curves of long-lived and short-lived short GRBs observed by *Swift* XRT and GRB 111117A (red). The *Chandra* data point of GRB 111117A is shown in red filled circle. The long-lived short GRBs included in this figure are GRB 050724, GRB 051221A, GRB 051227, GRB 060313, GRB 061006, GRB 061201, GRB 061210, GRB 070714B, GRB 070724A, GRB 070809, GRB 071227, GRB 080123, GRB 080426, GRB 090426, GRB 090510, GRB 090607, GRB 090621B, and GRB 091109B. The short-lived short GRBs included in this figure are GRB 050509B, GRB 050813, GRB 051210, GRB 060502B, GRB 060801, GRB 061217, GRB 070429B, GRB 080503, GRB 080702A, GRB 080905A, GRB 080919, GRB 081024A, and GRB 081226A.

(A color version of this figure is available in the online journal.)

it difficult to investigate whether the source is extended or not, the optical flux of the source is constant between 7 hr and 14 days after the burst at a level of $\sim$1.1 μJy (bottom panel of Figure 6). Using the formula provided by Bloom et al. (2002), the probability of finding an unrelated galaxy of the R magnitude of $\sim$23.3 with the distance of 1.″0 is 0.8%. We also investigate the chance probabilities of the three nearby objects. The probabilities of those objects are between 24% and 42% which are significantly larger than that of the host candidate. Although the chance probability of the host candidate is non-negligible, the chance of a misidentification of the host galaxy is reasonably small. Therefore, we conclude that the source detected in the K, J, z, i, r, g, and R bands is the host galaxy of GRB 111117A (Figure 7).

To estimate the redshift of the host galaxy, we perform a spectral energy density (SED) fit with the stellar population model of Maraston (2005). We use the single stellar population (SSP) models with a Salpeter initial mass function (Salpeter 1955), solar metallicity which ranges from 0.005 $Z_{\odot}$ to 3.5 $Z_{\odot}$ (0.005, 0.02, 0.5, 1.0, 2.0, and 3.5 $Z_{\odot}$), and a red or blue horizontal branch morphology. A total number of 269 SED templates ranging in stellar age from 10 Myr to 15 Gyr was applied. The Bayesian Photometric Redshift software (BPZ; Benítez 2000) is used to fit the data in g, r, and i bands (GTC), z band (GMG), J band (CFHT), and K band (UKIRT) with those SED templates. We find that the best-fit SED template corresponds to a solar metallicity, a red horizontal branch morphology, and the luminosity-weighted mean stellar age of 0.1 Gyr with a redshift of $1.36^{+0.45}_{-1.18}$. Our best-fit SED template of SSP model with a solar metallicity and a red horizontal branch matches well with other short GRB hosts studied by Leibler & Berger (2010). As seen in Figure 8 (top), there is a less significant low redshift solution ($z < 0.25$). We find that this low redshift solution is coming from the template with the young stellar age of $\sim$10 Myr. As we will discuss in Section 7, it is unlikely that the host galaxy has the stellar age of $\sim$10 Myr. Therefore, to constrain the redshift better, we focus on 41 SED templates with solar metallicity and a red horizontal branch morphology with stellar age from 20 Myr to 15 Gyr. The signal-to-noise is low, and there are no clear absorption or emission line features in the spectrum. The continuum is consistent with the best-fit SED template. The bottom panel of Figure 8 shows the posterior probability distribution of the estimated redshift for this SED fit. No low redshift solution is evident in the probability distribution. We find the best estimated redshift to

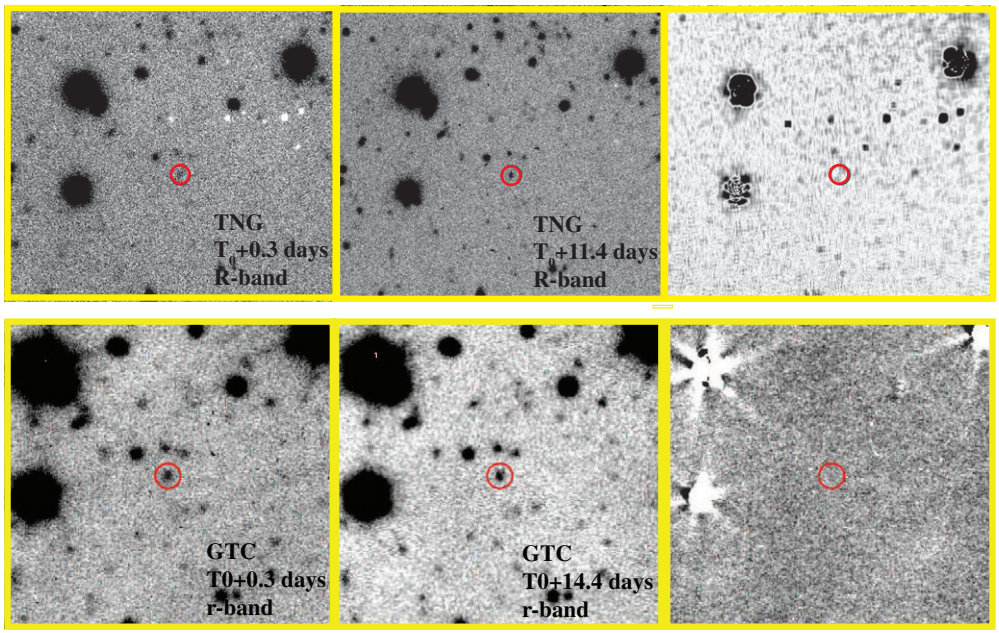

Figure 5. Deep optical TNG (R; 1.′4 × 1.′2) and GTC (r; 1.′1 × 1.′0) images of two epochs. The right panel shows the subtracted image of the first and second epoch. No significant residuals are seen in both TNG and GTC subtracted images at the host location (red circle).

(A color version of this figure is available in the online journal.)

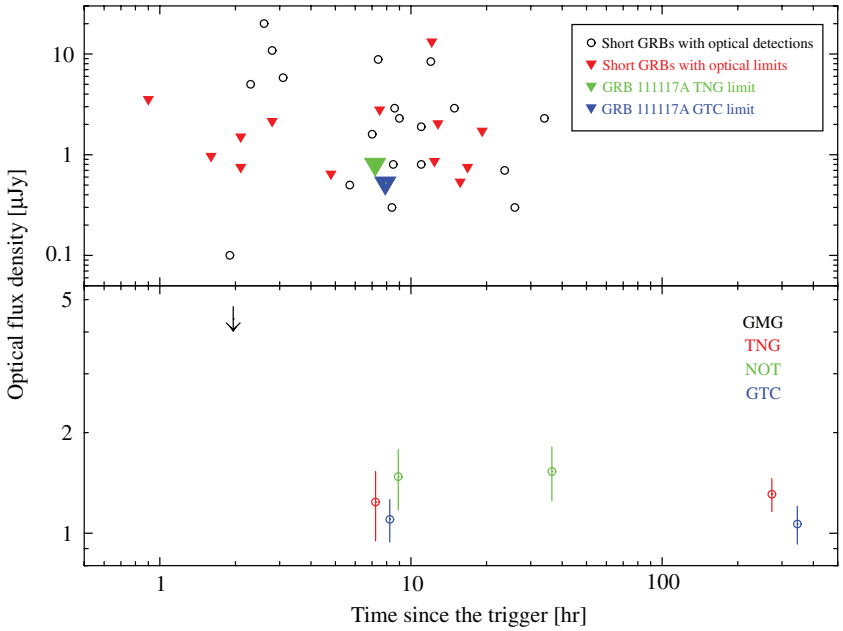

Figure 6. Top: optical fluxes of the first optical detection (black circle) or an upper limit (filled triangle) of short GRBs (Berger 2010) is shown as a function of the trigger time. The TNG and GTC upper limits of the optical afterglow of GRB 111117A are shown in green and blue filled triangle. Bottom: optical light curves of GRB 111117A in *R* and *r* band are shown. The plot includes *R* band measurement from GMG, TNG, and NOT, and also the *r* band measurement from GTC.

(A color version of this figure is available in the online journal.)

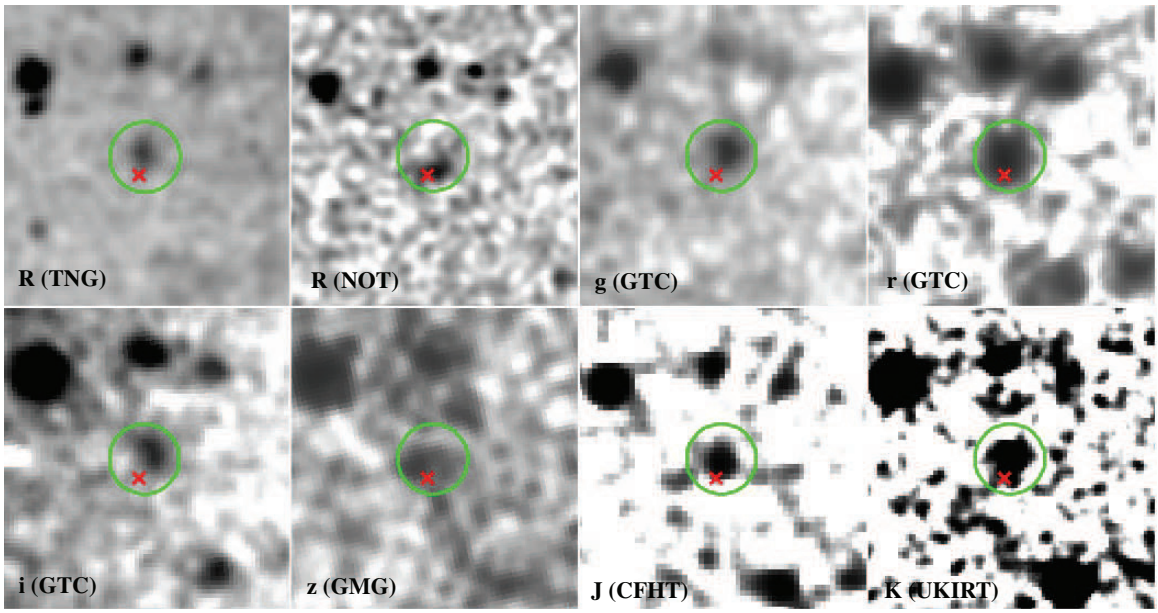

Figure 7. Multi-color images at the field of GRB 111117A. From left to right, and top to bottom, the images are TNG *R*, NOT *R*, GTC *g*, GTC *r*, GTC *i*, GMG *z*, CFHT *J*, and UKIRT *K*. The host galaxy is marked in a green circle. The X-ray afterglow position determined by *Chandra* is marked as a red cross. The image scale is $17'' \times 17''$. All the images are smoothed by the Gaussian function with 3 pixel radius.

(A color version of this figure is available in the online journal.)

be 1.31 (90% confidence interval $1.08 < z_{\rm ph} < 1.77$). The likelihood that the redshift is correct is 80% (reduced χ^2 of the fit is 0.65 with 2 dof). The best-fit SED template is the case with the luminosity weighted mean stellar age of 0.1 Gyr and a mass of $\sim 1 \times 10^9\ M_\odot$. Figure 9 shows the best-fit SED with the photometric data, and the GTC spectrum with an exposure time of 4×1800 s. GTC spectroscopy was performed with the R1000B grism, which has a central wavelength of 5510 Å and covers the spectral range between 3700 and 7000 Å with a resolution of ~1000 at 5500 Å. To investigate the likelihood of the host being a star-forming galaxy, we also examine the SED templates with an exponentially decaying star formation rate (Maraston et al. 2010), with an *e*-folding time of 0.1, 1 and 10 Gyr (stellar age ranges from 10 Myr to 15 Gyr). Although our *J* band data point shows a relatively poor agreement with the best-fit template with an *e*-folding time of 0.1 Gyr and the luminosity weighted mean stellar age of 0.3 Gyr, the fit is still acceptable (reduced $\chi^2 = 0.91$ with 2 dof). The best-fit redshift in this case is $1.18^{+0.61}_{-0.21}$. The fit becomes worse if the *e*-folding time gets larger. Therefore, our current data

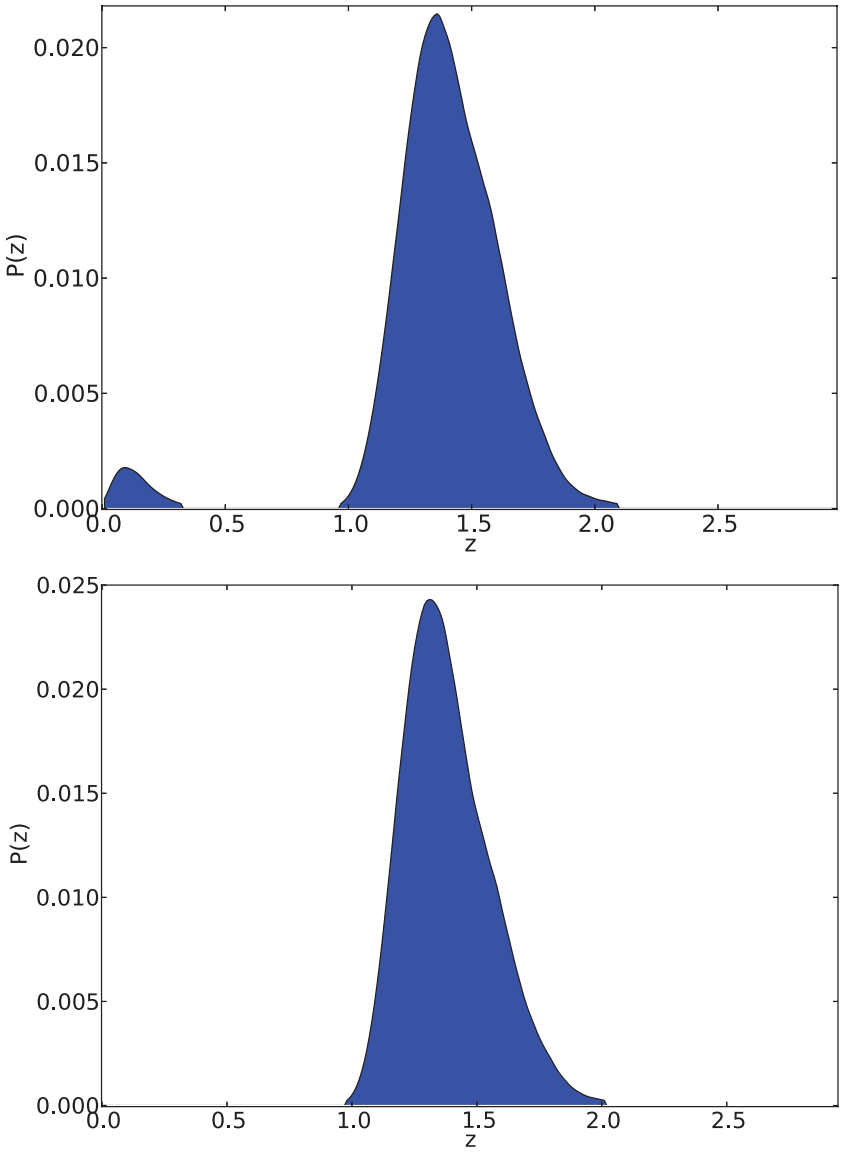

Figure 8. Top: posterior probability distribution of the photometric redshift by the SED fit of the host. All 269 SED templates are used. Bottom: posterior probability distribution of the photometric redshift of the host by 41 SED templates of a solar metallicity and a red horizontal branch morphology with stellar age from 20 Myr to 15 Gyr.

(A color version of this figure is available in the online journal.)

also support of an ∼0.1 Gyr post-starburst galaxy (see bottom panel of Figure 9). We also fitted the optical–NIR SED using the MAGPHYS package (de Cunha et al. 2008) to check the validity of the fitting result. The MAGPHYS fit includes an extinction parameter as a part of the fit, but performs the fitting at a given redshift. An exponentially decaying star formation rate is assumed. The redshifts were increased by a step of 0.05 from 0.8 to 1.5. We confirm that the returned χ^2 is the smallest in the range of the $z_{\rm ph}$ from the BPZ, and a moderate extinction of $A_V = 0.2$–0.5 mag is found. The best-fit solutions give the exponential time scale of about 1.5 Gyr, with the luminosity weighted mean stellar age (in r-band) of a few hundred Myr, and a stellar mass of a few times $10^9\ M_\odot$. These output values are consistent with the solutions derived with the photometric redshift. In summary, based on various SED template fits, we can conclude the following about the host galaxy: the redshift of the host is ∼1.3 regardless of the SED model and the host is either a star-forming galaxy of the luminosity weighted mean stellar age of 0.1 Gyr and a mass of $\sim 1 \times 10^9\ M_\odot$ or a post-starburst galaxy. Further deep J or Y band data are crucial to pin down the host properties.

A significant offset between the center of the host galaxy and the X-ray afterglow has been found for GRB 111117A. The center position of the host galaxy has been examined by running SExtractor on the second epoch of the GTC r image, our highest quality optical image. The best location of the host center is (R.A., Decl.) (J2000) = ($00^{\rm h}50^{\rm m}46\overset{\rm s}{.}258$, $+23^\circ00'40\overset{''}{.}97$). The position moves by less than half a pixel ($<0\overset{''}{.}13$) by changing the detection threshold of SExtractor from 1.5σ to 3σ. Therefore, the projected offset between the center of the host galaxy and the X-ray afterglow is $1\overset{''}{.}0$ (δR.A. = $0\overset{''}{.}083$ and δDecl. = $-0\overset{''}{.}990$; see Figure 7). Taking into account the statistical error in the X-ray afterglow position of $0\overset{''}{.}18$ and the statistical error of the host center location of $0\overset{''}{.}13$, we estimate the offset with its error to be 1.0 ± 0.2 arcsec, which corresponding to a distance of 8.4 ± 1.7 kpc at a redshift of $z = 1.31$.

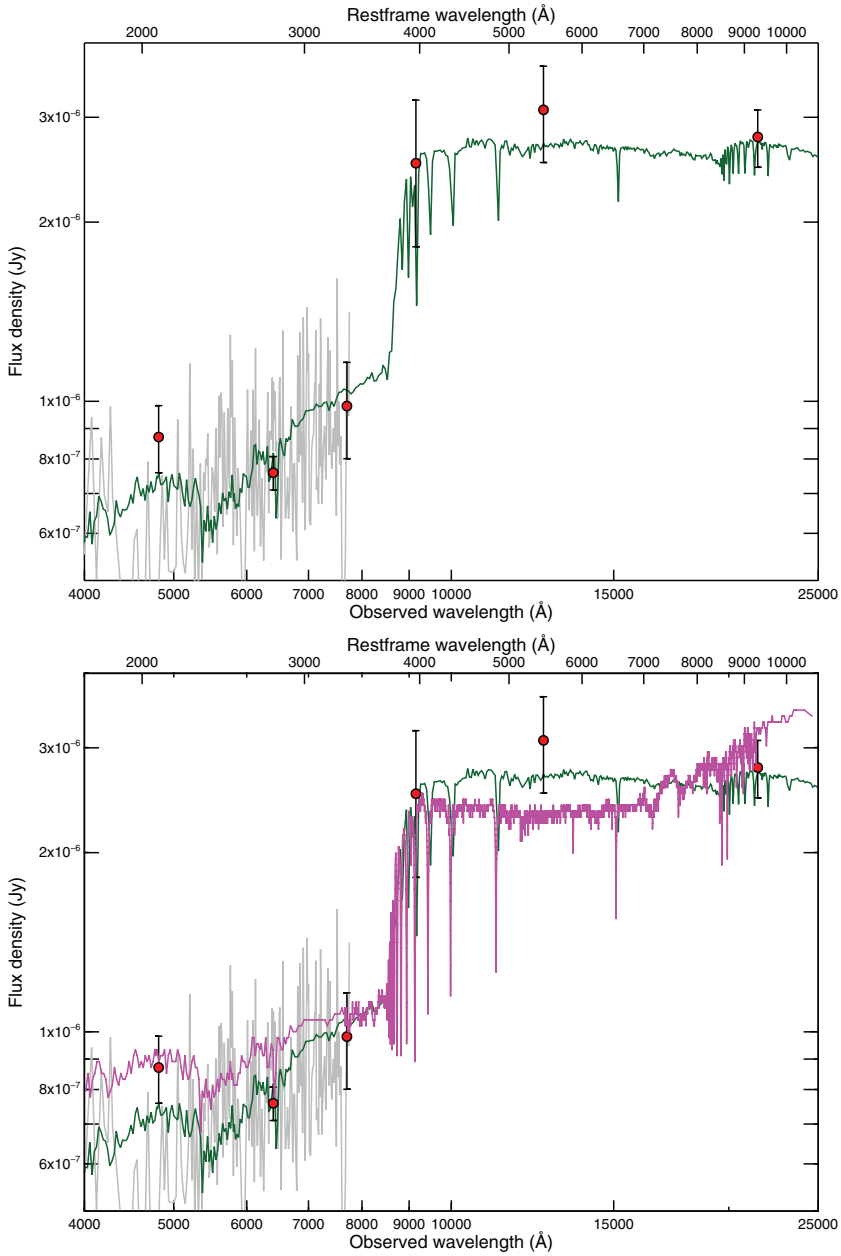

Figure 9. Top: the SED fit to the photometric data (g, r, i, z, J, and K) using the templates of the single stellar populations model (Maraston 2005). The GTC spectrum is shown in gray. Bottom: the best-fit SED template of the ∼0.1 Gyr post-starburst galaxy is overlaid in magenta.
(A color version of this figure is available in the online journal.)

7. DISCUSSION

Our photometric redshift of $1.31^{+0.46}_{-0.23}$ (90% confidence) for the host galaxy of GRB 111117A is realistic for the following reasons. First, by plotting the observed r AB magnitude ($r_{\rm AB}$) of the host galaxies of short GRBs as a function of redshift (Berger 2009), we find that the relatively faint magnitude of the host galaxy, $r_{\rm AB} = 24.20 \pm 0.07$, is located at the redshift range of >0.5 (Figure 10). Second, we find that the less significant low redshift solution ($z < 0.25$) in the photometric redshift estimation (Figure 8) is coming from the templates with the unrealistic young stellar ages of ∼10 Myr. At $z = 0.25$, if the galaxy is star forming, there would be a chance of seeing emissions of [O II], H-β, and [O III] in the optical spectrum, yet, we see none of those lines in the GTC spectrum. Furthermore, ∼10 Myr is in general too young for a whole galaxy, as opposed to a specific star forming region. Therefore the low redshift solution for the photometric redshift is unlikely to be the case of GRB 111117A. Therefore, hereafter, we will discuss the rest-frame properties of GRB 111117A using our best photometric redshift of 1.31.

Assuming the redshift of 1.31, the isotropic equivalent γ-ray energy ($E_{\gamma,\rm iso}$) which is integrated from 1 keV to 10 MeV in the rest frame is $3.4^{+5.7}_{-1.5} \times 10^{51}$ erg. The peak energy at the rest-frame ($E^{\rm src}_{\rm peak}$) is 945^{+455}_{-310} keV. The 90% errors in $E_{\gamma,\rm iso}$ and $E^{\rm src}_{\rm peak}$ are taking into account not only a statistical error but also an uncertainty in the estimated redshift. As shown in Figure 11, the $E_{\gamma,\rm iso}$ of GRB 111117A is located at the high end of the $E_{\gamma,\rm iso}$ distribution of short GRBs and at the low end of the $E_{\gamma,\rm iso}$ distribution of long GRBs. Relatively low $E_{\gamma,\rm iso}$ and high $E^{\rm src}_{\rm peak}$ compared to those of long GRBs make GRB 111117A

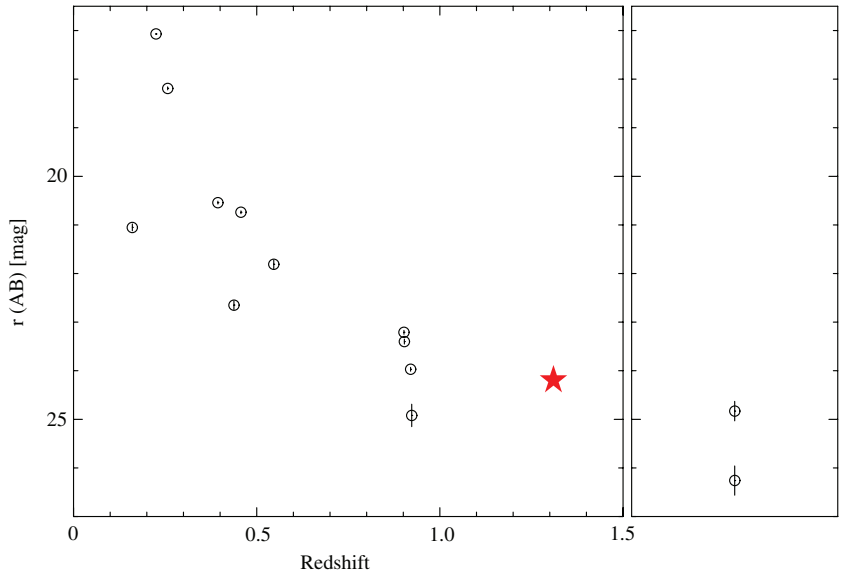

Figure 10. Magnitude of the short GRB hosts as a function of redshift. The right panel shows the magnitude of the hosts without a confirmed redshift. GRB 111117A ($z = 1.31$) is shown as a red star.

(A color version of this figure is available in the online journal.)

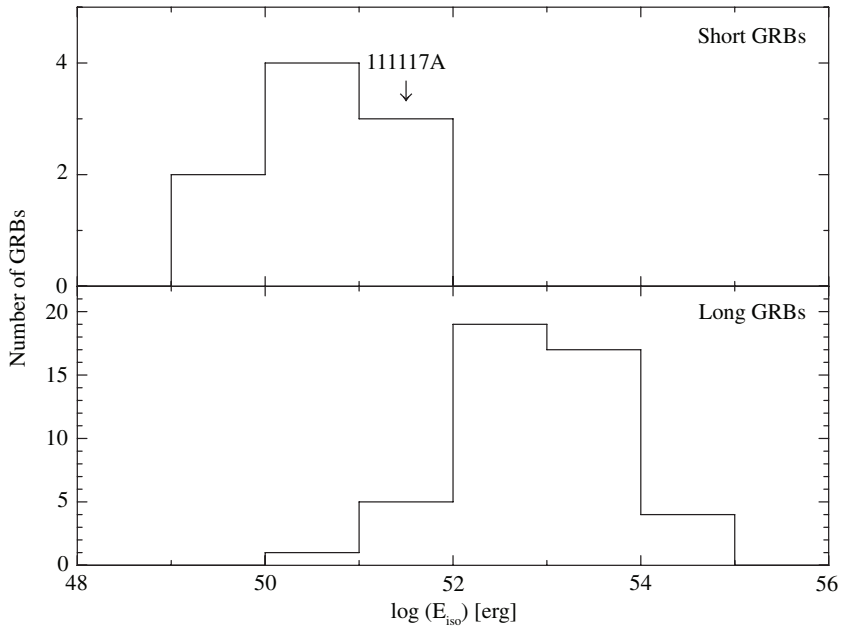

Figure 11. Comparison of $E_{\rm iso}$ between short (upper panel) and long (lower panel) GRBs. The short GRB $E_{\rm iso}$ values are from Berger (2010) (short GRBs with detected afterglows and coincident host galaxies), and the long GRB $E_{\rm iso}$ values are from Nava et al. (2012) (only *Swift* long GRBs). GRB 111117A (3.4×10^{51} erg) is located at the high end of $E_{\rm iso}$ distribution of short GRBs.

inconsistent with the $E^{\rm src}_{\rm peak}$-$E_{\gamma,{\rm iso}}$ (Amati) relation (Amati et al. 2002). This characteristic is consistent with being a short GRB because most of the short GRBs are well known outliers of the Amati relation (Amati 2006; Nava et al. 2012).

The optical-to-X-ray spectral index (Jakobsson et al. 2004),

$$\beta_{\rm OX}(\equiv \log\{f_\nu(R)/f_\nu(3\,{\rm keV})\}/\log(\nu_{3\,{\rm keV}}/\nu_{\rm R})),$$

is estimated to be $\lesssim$0.78 using the same definition on the X-ray flux density at 3 keV measured at 11 hr after the burst, and the optical afterglow limit based on the GTC r band. This upper limit of $\beta_{\rm OX}$ is within the allowed range of the standard afterglow model between 0.5 to 1.25. Furthermore, according to Margutti et al. (2012), the optical and the radio afterglow limit is consistent with the external shock model (Granot & Sari 2002) for a small number density ($n \lesssim 0.01$–$0.2\,{\rm cm}^{-3}$). However, there is a possibility that a significant amount of the optical afterglow flux was extinguished by the host galaxy. When we fit the X-ray afterglow spectrum to a power-law model with the intrinsic absorption at $z = 1.31$, the intrinsic $N_{\rm H}$ is estimated to be $7.2^{+0.7}_{-0.5} \times 10^{21}$ cm^{-2}. Assuming a host extinction law similar to the Milky Way, A_V is 4.1 mag (Predehl & Schmitt 1995). Therefore, a significant amount of extinction in the optical flux is expected from the X-ray column density measurement. On the other hand, it is still not clear whether it is possible to have such high extinction at the outskirts of the host where the X-ray afterglow is indicated. Moreover, the amount of extinction which we derived from the SED fit of the host is $A_V = 0.2$–0.5 mag

(see Section 6). At this stage, the origin of the large column density seen in the X-ray afterglow of GRB 111117A remains puzzling.

The projected offset between the afterglow location and the host galaxy center is 8.4 ± 1.7 kpc using the estimated redshift of 1.31. Although this offset is larger than the median projected offset of $\sim$5 kpc for previously studied short GRBs (Fong et al. 2010), it is within the offset distribution of short GRBs. Using the projected offset of $r = 8.4$ kpc and the stellar age of $\tau = 0.1$ Gyr, the minimum kick velocity, $v = r/\tau$, is estimated to be $\approx$80 km s^{-1}. The estimated kick velocity is similar to or possibly larger than the inferred kick velocity of GRB 060502B (Bloom et al. 2007). Using the typical age of 1–10 Gyr in the early-type short GRB hosts such as GRB 050509B, GRB 070809 and GRB 090515 (Bloom et al. 2006; Berger 2010), the minimum kick velocity is estimated to be $\approx$1–8 km s^{-1}.

In this paper, we have reported the prompt emission, the afterglow, and the host galaxy properties of short GRB 111117A. The prompt emission observed by the *Swift* BAT and the *Fermi* GBM showed (1) a short duration, (2) no extended emission, (3) no measurable spectral lag, and (4) a hard spectrum. All those properties can securely classify this burst as a short GRB. Although the optical afterglow has not been detected by our deep observations by TNG and GTC, our rapid *Chandra* ToO observation provides a subarcsecond position of the afterglow in X-rays. This *Chandra* position is crucial to identify the host galaxy and also to measure the significant offset of 1.″0 between the host center and the afterglow location. Our deep near-infrared to optical photometry data of GMG, TNG, NOT, GTC, UKIRT, and CFHT enable us to estimate the redshift of the host to 1.31. The observation of GRB 111117A suggests that X-rays are more promising than optical to locate short GRBs with subarcsecond accuracy. Combining the subarcsecond afterglow position in the X-ray and the deep optical images from the ground telescopes, we successfully investigate the host properties of GRB 111117A even without an optical afterglow. Rapid *Chandra* ToO observations of short GRBs are still key to increasing the *golden* sample of short GRBs with redshifts to pin down their nature.

We would like to thank the anonymous referee for comments and suggestions that materially improved the paper. This work made use of data supplied by the UK *Swift* Science Data Centre at the University of Leicester. This work is based on observations using the United Kingdom Infrared Telescope, which is operated by the Joint Astronomy Centre on behalf of the Science and Technology Facilities Council of the U.K. with a partial support by *Swift* mission (e.g., *Swift* Cycle 7 GI grant NNX12AE75G) and the Gran Telescopio Canarias (GTC), installed in the Spanish Observatorio del Roque de los Muchachos of the Instituto de Astrofísica de Canarias, on the island of La Palma. The Dark Cosmology Centre is funded by the Danish National Research Foundation. This research is partly based on observations made with the Nordic Optical Telescope, operated on the island of La Palma jointly by Denmark, Finland, Iceland, Norway, and Sweden, in the Spanish Observatorio del Roque de los Muchachos of the Instituto de Astrofísica de Canarias. This work was supported by *Chandra* Cycle 13 grant GO2-13084X. The research activity of A.d.U.P., C.C.T., R.S.R., and J.G. is supported by Spanish research projects AYA2011-24780/ESP, AYA2009-14000-C03-01/ESP and AYA2010-21887-C04-01. G.L. is supported by the Swedish Research Council through grant No. 623-2011-7117. K.V. is grateful to the Hungarian Science Research Program (OTKA) for support under the grant K-81421. This work is supported by the "Lendület" Young Researchers' Program of the Hungarian Academy of Sciences. H.K. acknowledges the support from the European Commission under the Marie Curie IEF Programme in FP7. M.I. and Y.J. were supported by the Creative Research Initiative program, No. 2010-0000712, of the National Research Foundation of Korea (NRFK) funded by the Korean government (MEST).

REFERENCES

Alard, C., & Lupton, R. H. 1998, ApJ, 503, 325
Amati, L. 2006, MNRAS, 372, 233
Amati, L., Frontera, F., Tavani, M., et al. 2002, A&A, 390, 81
Andersen, M. I., de Ugarte Postigo, A., Leloudas, G., & Fynbo, J. P. U. 2011, GCN Circ., 12563
Band, D. L., Matteson, J., Ford, L., et al. 1993, ApJ, 413, 281
Barthelmy, S. D., Barbier, L. M., Cummings, J. R., et al. 2005, SSRv, 120, 143
Belczynski, K., Perna, R., Bulik, T., et al. 2006, ApJ, 648, 1110
Benítez, N. 2000, ApJ, 536, 571
Berger, E. 2009, ApJ, 690, 231
Berger, E. 2010, ApJ, 722, 1946
Berger, E., Fox, D. B., Price, P. A., et al. 2007, ApJ, 664, 1000
Bertin, E., & Arnouts, S. 1996, A&AS, 117, 393
Bloom, J. S., Kulkarni, S. R., & Djorgovski, S. G. 2002, AJ, 123, 1111
Bloom, J. S., Sigurdsson, S., & Pols, O. R. 1999, MNRAS, 305, 763
Bloom, J. S., Perley, D. A., Chen, H.-W., et al. 2007, ApJ, 654, 878
Bloom, J. S., Prochaska, J. X., Pooley, D., et al. 2006, ApJ, 638, 354
Bromberg, O., Nakar, E., Piran, T., & Sari, R. 2012, ApJ, 749, 110
Burrows, S. D., Hill, J. E., Nousek, J. A., et al. 2005, SSRv, 120, 165
Church, R. P., Levan, A. J., Davies, M. B., & Tanvir, N. 2011, MNRAS, 413, 2004
Covino, S., Malesani, D., Israel, G. L., et al. 2006, A&A, 447, L5
Cucchiara, A., & Cenko, S. B. 2011, GCN Circ., 12567
de Cunha, E., Charlot, S., & Elbaz, D. 2008, MNRAS, 388, 1595
de Ugarte Postigo, A., Castro-Tirado, A. J., Guziy, S., et al. 2006, ApJL, 648, L83
Eichler, D., Livio, M., Piran, T., & Schramm, D. M. 1989, Natur, 340, 126
Evans, P. A., Beardmore, A. P., Page, K. L., et al. 2007, A&A, 469, 379
Evans, P. A., Beardmore, A. P., Page, K. L., et al. 2009, MNRAS, 397, 1177
Feng, H., & Kaaret, P. 2008, ApJ, 675, 1067
Foley, S., Zauderer, B. A., & Berger, E. 2011, GCN Circ., 12573
Fong, W., Berger, E., & Fox, D. B. 2010, ApJ, 708, 9
Fong, W., Berger, E., Margutti, R., et al. 2012, ApJ, 756, 189
Fong, W., Sanders, N., Milisavljevic, D., & Berger, E. 2011, GCN Circ., 12566
Fryer, C. L., Woosley, S. E., & Hartmann, D. H. 1999, ApJ, 526, 152
Gehrels, N., Chincarini, G., Giommi, P., et al. 2004, ApJ, 611, 1005
Ghirlanda, G., Nava, L., Ghisellini, G., Celotti, A., & Firmani, C. 2009, A&A, 496, 585
Granot, J., & Sari, R. 2002, ApJ, 568, 820
Grindlay, J., Portegies Zwart, S., & McMillan, S. 2006, NatPh, 2, 116
Jakobsson, P., Hjorth, J., Fynbo, P. U., et al. 2004, ApJL, 617, L21
Kalberla, P. M. W., Burton, W. B., Hartmann, D., et al. 2005, A&A, 440, 775
Kann, D. A., Klose, S., Zhang, B., et al. 2011, ApJ, 734, 96
Kopač, D., D'Avanzo, P., Melandri, A., et al. 2012, MNRAS, 424, 2392
Kouveliotou, C., Meegan, C. A., Fishman, G. J., et al. 1993, ApJL, 413, L101
Kumar, P., & Panaitescu, A. 2000, ApJL, 541, L51
Leibler, C. N., & Berger, E. 2010, ApJ, 725, 1202
Levan, A. J., Tanvir, N. R., Fruchter, A. S., et al. 2006, ApJL, 648, L9
Levesque, E. M., Bloom, J. S., Butler, N. R., et al. 2010, MNRAS, 401, 963
Lü, H., Liang, E.-W., Zhang, B.-B., & Zhang, B. 2010, ApJ, 725, 1965
Mangano, V., Baumgartner, W. H., Beardmore, A. P., et al. 2011, GCN Circ., 12559
Maraston, C. 2005, MNRAS, 362, 799
Maraston, C., Pforr, J., Renzini, A., et al. 2010, MNRAS, 407, 830
Margutti, R., Berger, E., Fong, W., et al. 2012, ApJ, 756, 63
Meegan, C. A., Giselher, L., Bhat, P. N., et al. 2009, ApJ, 702, 791
Melandri, A., Fugazza, D., Covino, S., & Palazzi, E. 2011a, GCN Circ., 12570
Melandri, A., Sbarufatti, B., Stratta, G., et al. 2011b, GCN Circ., 12565
Narayan, R., Paczynski, B., & Piran, T. 1992, ApJL, 395, L83
Nava, L., Salvaterra, R., Ghirlanda, G., et al. 2012, MNRAS, 421, 1256
Nissanke, S., Holz, D. E., Hughes, S. A., et al. 2010, ApJ, 725, 496
Norris, J. P., & Bonnell, J. T. 2006, ApJ, 643, 266
Norris, J. P., Gehrels, N., & Scargle, J. D. 2011, ApJ, 735, 23

Nysewander, M., Fruchter, A. S., & Pe'er, A. 2009, ApJ, 701, 824
Oates, S. R., & Mangano, V. 2011, GCN Circ., 12569
Ohno, M., Fukazawa, Y., Takahashi, T., et al. 2008, PASJ, 60, 361
Paczynski, B. 1991, AcA, 41, 257
Predehl, P., & Schmitt, J. H. M. M. 1995, A&A, 293, 889
Prochaska, J. X., Bloom, J. S., Chen, H.-W., et al. 2006, ApJ, 642, 989
Rezzolla, L., Giacomazzo, B., Baiotti, L., et al. 2011, ApJL, 732, L6
Ricker, G. R., Atteia, J.-L., Crew, G. B., et al. 2003, in AIP Conf. Proc. 662, Gamma-Ray Burst and Afterglow Astronomy 2001, ed. G. R. Ricker & R. K. Vanderspek (Melville, NY: AIP), 3
Roming, P. W. A., Kennedy, T. E., Mason, K. O., et al. 2005, SSRv, 120, 95
Rosswog, S. 2005, ApJ, 634, 1202
Sakamoto, T., Barthelmy, S. D., Baumgartner, W. H., et al. 2011a, ApJS, 195, 2
Sakamoto, T., Barthelmy, S. D., Baumgartner, W. H., et al. 2011b, GCN Circ., 12562
Sakamoto, T., & Gehrels, N. 2009, in AIP Conf. Proc. 1133, Gamma-Ray Bursts, 6th Huntsville Symposium, ed. C. Meegan, N. Gehrels, & C. Kouveliotou (Melville, NY: AIP), 112
Sakamoto, T., Troja, E., Gehrels, N., et al. 2011c, GCN Circ., 12580
Salpeter, E. E. 1955, ApJ, 121, 161
Salvaterra, R., Devecchi, B., Colpi, M., & D'Avanzo, P. 2010, MNRAS, 406, 1248
Schlegel, D. J., Finkbeiner, D. P., & Davis, M. 1998, ApJ, 500, 525
Schmidl, S., Rossi, A., Kann, D. A., & Greiner, J. 2011, GCN Circ., 12568
Thöne, C. C., Campana, S., Lazzati, D., et al. 2011, MNRAS, 414, 479
Troja, E., King, A. R., O'Brien, P. T., Lyons, N., & Cusumano, G. 2008, MNRAS, 385, L10
Woosley, S. E., & Bloom, J. S. 2006, ARA&A, 44, 507
Xin, L., Liang, E.-W., Wei, J.-Y., et al. 2011, MNRAS, 410, 27
Zhao, X.-H., Xu, D., Mao, J.-R., & Bai, J.-M. 2011, GCN Circ., 12560